

# The angular power spectrum measurement of the Galactic synchrotron emission in two fields of the TGSS survey

Samir Choudhuri<sup>1,2\*</sup>, Somnath Bharadwaj<sup>2</sup>, Sk. Saiyad Ali<sup>3</sup>, Nirupam Roy<sup>4</sup>  
Huib. T. Intema<sup>5</sup> and Abhik Ghosh<sup>6,7</sup>

<sup>1</sup> National Centre For Radio Astrophysics, Post Bag 3, Ganeshkhind, Pune 411 007, India

<sup>2</sup> Department of Physics, & Centre for Theoretical Studies, IIT Kharagpur, Kharagpur 721 302, India

<sup>3</sup> Department of Physics, Jadavpur University, Kolkata 700032, India

<sup>4</sup> Department of Physics, Indian Institute of Science, Bangalore 560012, India

<sup>5</sup> Leiden Observatory, Leiden University, Niels Bohrweg 2, NL-2333CA, Leiden, The Netherlands

<sup>6</sup> Department of Physics and Astronomy, University of the Western Cape, Robert Sobukwe Road, Bellville 7535, South Africa

<sup>7</sup> SKA SA, The Park, Park Road, Pinelands 7405, South Africa

## ABSTRACT

Characterizing the diffuse Galactic synchrotron emission at arcminute angular scales is needed to reliably remove foregrounds in cosmological 21-cm measurements. The study of this emission is also interesting in its own right. Here, we quantify the fluctuations of the diffuse Galactic synchrotron emission using visibility data for two of the fields observed by the TIFR GMRT Sky Survey (TGSS). We have used the 2D Tapered Gridded Estimator (TGE) to estimate the angular power spectrum ( $C_\ell$ ) from the visibilities. We find that the sky signal, after subtracting the point sources, is likely dominated by the diffuse Galactic synchrotron radiation across the angular multipole range  $240 \leq \ell \lesssim 500$ . We present a power law fit,  $C_\ell = A \times \left(\frac{1000}{\ell}\right)^\beta$ , to the measured  $C_\ell$  over this  $\ell$  range. We find that  $(A, \beta)$  have values  $(356 \pm 109 \text{ mK}^2, 2.8 \pm 0.3)$  and  $(54 \pm 26 \text{ mK}^2, 2.2 \pm 0.4)$  in the two fields. For the second field, however, there is indication of a significant residual point source contribution, and for this field we interpret the measured  $C_\ell$  as an upper limit for the diffuse Galactic synchrotron emission. While in both fields the slopes are consistent with earlier measurements, the second field appears to have an amplitude which is considerably smaller compared to similar measurements in other parts of the sky.

**Key words:** methods: statistical, data analysis - techniques: interferometric- cosmology: diffuse radiation

## 1 INTRODUCTION

Observations of the redshifted 21-cm signal from the Epoch of Reionization (EoR) contain a wealth of cosmological and astrophysical information (Bharadwaj & Ali 2005; Furlanetto et al. 2006; Morales & Wyithe 2010; Pritchard & Loeb 2012). The Giant Metrewave Radio Telescope (GMRT, Swarup et al. 1991) is currently functioning at a frequency band which corresponds to the 21-cm signal from this epoch. Several ongoing and future experiments such as the Donald C. Backer Precision Array to Probe the Epoch of Reionization (PAPER, Parsons et al. 2010), the Low Frequency Array (LOFAR, van Haarlem et al. 2013), the Murchison Wide-field Array (MWA, Bowman et al. 2013), the Square Kilometer Ar-

ray (SKA1 LOW, Koopmans et al. 2015) and the Hydrogen Epoch of Reionization Array (HERA, Neben et al. 2016) are aiming to measure the EoR 21-cm signal. The EoR 21-cm signal is overwhelmed by different foregrounds which are four to five orders of magnitude stronger than the expected 21-cm signal (Shaver et al. 1999; Ali et al. 2008; Ghosh et al. 2011a,b). Accurately modelling and subtracting the foregrounds from the data are the main challenges for detecting the EoR 21-cm signal. The diffuse Galactic synchrotron emission (hereafter, DGSE) is expected to be the most dominant foreground at 10 arcminute angular scales after point source subtraction at 10-20 mJy level (Bernardi et al. 2009; Ghosh et al. 2012; Iacobelli et al. 2013). A precise characterization and a detailed understanding of the DGSE is needed to reliably remove foregrounds in 21-cm experiments. In this paper, we

\* Email:samir11@phy.iitkgp.ernet.in

characterize the DGSE at arcminute angular scales which are relevant for the cosmological 21-cm studies.

The study of the DGSE is also important in its own right. The angular power spectrum ( $C_\ell$ ) of the DGSE quantifies the fluctuations in the magnetic field and in the electron density of the turbulent interstellar medium (ISM) of our Galaxy (e.g. Waelkens et al. 2009; Lazarian & Pogosyan 2012; Iacobelli et al. 2013).

There are several observations towards characterizing the DGSE spanning a wide range of frequency. Haslam et al. (1982) have measured the all sky diffuse Galactic synchrotron radiation at 408 MHz. Reich (1982) and Reich & Reich (1988) have presented the Galactic synchrotron maps at a relatively higher frequency (1420 MHz). Using the 2.3 GHz Rhodes Survey, Giardino et al. (2001) have shown that the  $C_\ell$  of the diffuse Galactic synchrotron radiation behaves like a power law ( $C_\ell \propto \ell^{-\beta}$ ) where the power law index  $\beta = 2.43$  in the  $\ell$  range  $2 \leq \ell \leq 100$ . Giardino et al. (2002) have found that the value of  $\beta$  is 2.37 for the 2.4 GHz Parkes Survey in the  $\ell$  range  $40 \leq \ell \leq 250$ . The  $C_\ell$  measured from the *Wilkinson Microwave Anisotropy Probe* (WMAP) data show a slightly lower value of  $\beta$  ( $C_\ell \propto \ell^2$ ) for  $\ell < 200$  (Bennett et al. 2003). Bernardi et al. (2009) have analysed 150 MHz Westerbork Synthesis Radio Telescope (WSRT) observations to characterize the statistical properties of the diffuse Galactic emission and find that

$$C_\ell = A \times \left(\frac{1000}{\ell}\right)^\beta \text{mK}^2 \quad (1)$$

where  $A = 253 \text{ mK}^2$  and  $\beta = 2.2$  for  $\ell \leq 900$ . Ghosh et al. (2012) have used GMRT 150 MHz observations to characterize the foregrounds for 21-cm experiments and find that  $A = 513 \text{ mK}^2$  and  $\beta = 2.34$  in the  $\ell$  range  $253 \leq \ell \leq 800$ . Recently, Iacobelli et al. (2013) present the first LOFAR detection of the DGSE around 160 MHz. They reported that the  $C_\ell$  of the foreground synchrotron fluctuations is approximately a power law with a slope  $\beta \approx 1.8$  up to angular multipoles of 1300.

In this paper we study the statistical properties of the DGSE using two fields observed by the TIFR GMRT Sky Survey (TGSS<sup>1</sup>; Sirothia et al. 2014). We have used the data which was calibrated and processed by Intema et al. (2016). We have applied the Tapered Gridded Estimator (TGE; Choudhuri et al. 2016, hereafter Paper I) to the residual data to measure the  $C_\ell$  of the background sky signal after point source subtraction. The TGE suppresses the contribution from the residual point sources in the outer region of the telescope’s field of view (FoV) and also internally subtracts out the noise bias to give an unbiased estimate of  $C_\ell$  (Choudhuri et al. 2016a). For each field we are able to identify an angular multipole range where the measured  $C_\ell$  is likely dominated by the DGSE, and we present power law fits for these.

## 2 DATA ANALYSIS

The TGSS survey contains 2000 hours of observing time divided on 5336 individual pointings on an approximate hexagonal grid. The observing time for each field is about

15 minutes. For the purpose of this paper, we have used only two data sets for two fields located at Galactic coordinates ( $9^\circ, +10^\circ$ ; **Data1**) and ( $15^\circ, -11^\circ$ ; **Data2**). We have selected these fields because they are close to the Galactic plane, and also the contributions from the very bright compact sources are much less in these fields. The central frequency of this survey is 147.5 MHz with an instantaneous bandwidth of 16.7 MHz which is divided into 256 frequency channels. All the TGSS raw data was analysed with a fully automated pipeline based on the SPAM package (Intema et al. 2009; Intema 2014). The operation of the SPAM package is divided into two parts: (a) *Pre-processing* and (b) *Main pipeline*. The Pre-processing step calculates good-quality instrumental calibration from the best available scans on one of the primary calibrators, and transfers these to the target field. In the Main pipeline the direction independent and direction dependent calibrations are calculated for each field, and the calibrated visibilities are converted into “CLEANed” deconvolved radio images. The off source rms noise ( $\sigma_n$ ) for the continuum images of these fields are 4.1 mJy/Beam and 3.1 mJy/Beam for **Data1** and **Data2** respectively, both values lie close to the median rms. noise of 3.5 mJy/Beam for the whole survey. The angular resolution of these observations is  $25'' \times 25''$ . This pipeline applies direction-dependent gains to image and subtract point sources to a  $S_c = 5\sigma_n$  flux threshold covering an angular region of radius  $\sim 1.5$  times the telescope’s FoV ( $3.1^\circ \times 3.1^\circ$ ), and also includes a few bright sources even further away. The subsequent analysis here uses the residual visibility data after subtracting out the discrete sources.

We have used the TGE to estimate  $C_\ell$  from the measured visibilities  $\mathcal{V}_i$  with  $\mathbf{U}_i$  referring to the corresponding baseline. As mentioned earlier, the TGE suppresses the contribution from the residual point sources in the outer region of the telescope’s FoV and also internally subtracts out the noise bias to give an unbiased estimate of  $C_\ell$  (details in Choudhuri et al. 2014, 2016a, Paper I). The tapering is introduced by multiplying the sky with a Gaussian window function  $\mathcal{W}(\theta) = e^{-\theta^2/\theta_w^2}$ . The value of  $\theta_w$  should be chosen in such a way that it cuts off the sky response well before the first null of the primary beam without removing too much of the signal from the central region. Here we have used  $\theta_w = 95'$  which is slightly smaller than  $114'$ , the half width at half maxima (HWHM) of the GMRT primary beam at 150 MHz. This is implemented by dividing the  $uv$  plane into a rectangular grid and evaluating the convolved visibilities  $\mathcal{V}_{cg}$  at every grid point  $g$

$$\mathcal{V}_{cg} = \sum_i \tilde{w}(\mathbf{U}_g - \mathbf{U}_i) \mathcal{V}_i \quad (2)$$

where  $\tilde{w}(\mathbf{U})$  is the Fourier transform of the taper window function  $\mathcal{W}(\theta)$  and  $\mathbf{U}_g$  refers to the baseline of different grid points. The entire data containing visibility measurements in different frequency channels that spans a 16 MHz bandwidth was collapsed to a single grid after scaling each baseline to the appropriate frequency.

The self correlation of the gridded and convolved visibilities (equation (10) and (13) of Paper I) can be written

<sup>1</sup> <http://tgss.ncra.tifr.res.in>

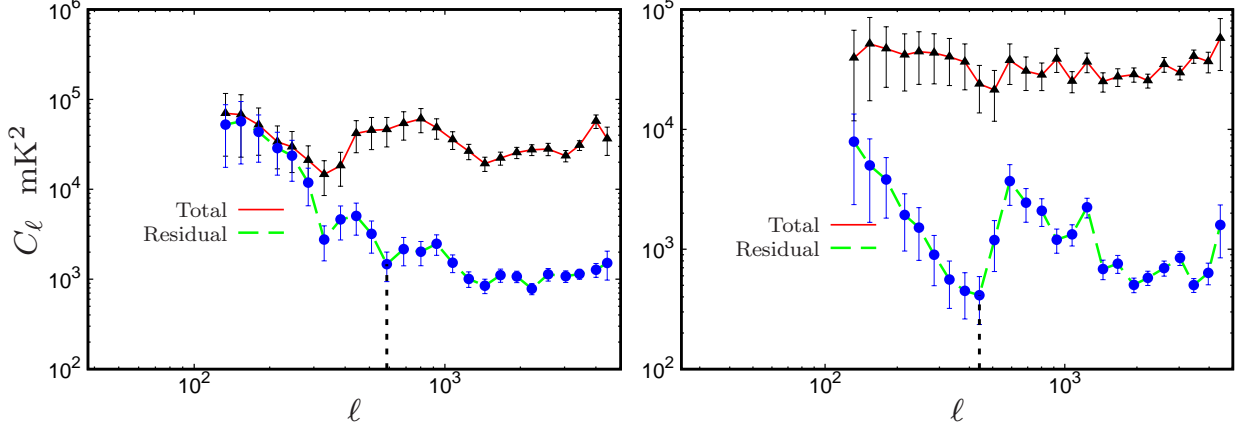


**Figure 1.** Estimated angular power spectra ( $C_\ell$ ) with  $1 - \sigma$  analytical error bars. The left and right panels are for **Data1** and **Data2** respectively. The upper and lower curves are before and after point source subtraction respectively. The vertical dotted lines in both the panels show  $\ell_{max}$  beyond which ( $\ell > \ell_{max}$ ) the residual  $C_\ell$  is dominated by the unsubtracted point sources.

as,

$$\langle |\mathcal{V}_{cg}|^2 \rangle = \left( \frac{\partial B}{\partial T} \right)^2 \int d^2U |\tilde{K}(\mathbf{U}_g - \mathbf{U})|^2 C_{2\pi U_g} + \sum_i |\tilde{w}(\mathbf{U}_g - \mathbf{U}_i)|^2 \langle |\mathcal{N}_i|^2 \rangle, \quad (3)$$

where,  $\left( \frac{\partial B}{\partial T} \right)$  is the conversion factor from brightness temperature to specific intensity,  $\mathcal{N}_i$  is the noise contribution to the individual visibility  $\mathcal{V}_i$  and  $\tilde{K}(\mathbf{U}_g - \mathbf{U})$  is an effective “gridding kernel” which incorporates the effects of (a) telescope’s primary beam pattern (b) the tapering window function and (c) the baseline sampling in the  $uv$  plane.

We have approximated the convolution in equation (3) as,

$$\langle |\mathcal{V}_{cg}|^2 \rangle = \left[ \left( \frac{\partial B}{\partial T} \right)^2 \int d^2U |\tilde{K}(\mathbf{U}_g - \mathbf{U})|^2 \right] C_{2\pi U_g} + \sum_i |\tilde{w}(\mathbf{U}_g - \mathbf{U}_i)|^2 \langle |\mathcal{N}_i|^2 \rangle, \quad (4)$$

under the assumption that the  $C_\ell$  ( $\ell = 2\pi |\mathbf{U}|$ ) is nearly constant across the width of  $\tilde{K}(\mathbf{U}_g - \mathbf{U})$ .

We define the Tapered Gridded Estimator (TGE) as

$$\hat{E}_g = M_g^{-1} \left( |\mathcal{V}_{cg}|^2 - \sum_i |\tilde{w}(\mathbf{U}_g - \mathbf{U}_i)|^2 |\mathcal{V}_i|^2 \right). \quad (5)$$

where  $M_g$  is the normalizing factor which we have calculated by using simulated visibilities corresponding to an unit angular power spectrum (details in Paper I). We have  $\langle \hat{E}_g \rangle = C_{\ell_g}$  *i.e.* the TGE  $\hat{E}_g$  provides an unbiased estimate of the angular power spectrum  $C_\ell$  at the angular multipole  $\ell_g = 2\pi U_g$  corresponding to the baseline  $\mathbf{U}_g$ . We have used the TGE to estimate  $C_\ell$  and its variance in bins of equal logarithmic interval in  $\ell$  (equations (19) and (25) in Paper I).

### 3 RESULTS AND CONCLUSIONS

The upper curves of the left and right panels of Figure 1 show the estimated  $C_\ell$  before point source subtraction for

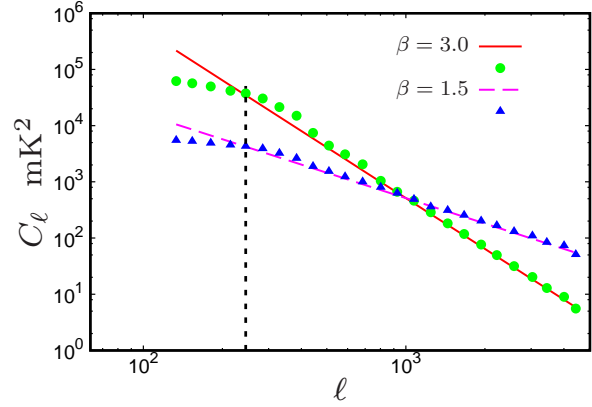


**Figure 2.** Comparison between the estimated  $C_\ell$  and the model  $C_\ell^M$  using simulation for **Data1**. The data points and the lines are for the estimated  $C_\ell$  and the input model  $C_\ell^M$  (with  $\beta = 1.5$  and 3) respectively. We see that the convolution is important in the range  $\ell < \ell_{min} = 240$  shown by the vertical dashed line and we have excluded this region from our subsequent analysis. The estimated  $C_\ell$  matches closely with  $C_\ell^M$  in the range  $\ell \geq \ell_{min}$  which we have used for our analysis.

**Data1** and **Data2** respectively. We find that for both the data sets the measured  $C_\ell$  is in the range  $10^4 - 10^5$   $\text{mK}^2$  across the entire  $\ell$  range. Model predictions (Ali et al. 2008) indicate that the point source contribution is expected to be considerably larger than the Galactic synchrotron emission across much of the  $\ell$  range considered here, however the two may be comparable at the smaller  $\ell$  values of our interest. Further, the convolution in equation (3) is expected to be important at small  $\ell$ , and it is necessary to also account for this. The lower curves of both the panels of Figure 1 show the estimated  $C_\ell$  after point source subtraction. We see that removing the point sources causes a very substantial drop in the  $C_\ell$  measured at large  $\ell$ . This clearly demonstrates that the  $C_\ell$  at these angular scales was dominated by the point sources prior to their subtraction. We further believe that after point source subtraction the  $C_\ell$  measured at large  $\ell$  continues to be dominated by the residual point sources which are below the threshold flux. The residual flux from imper-

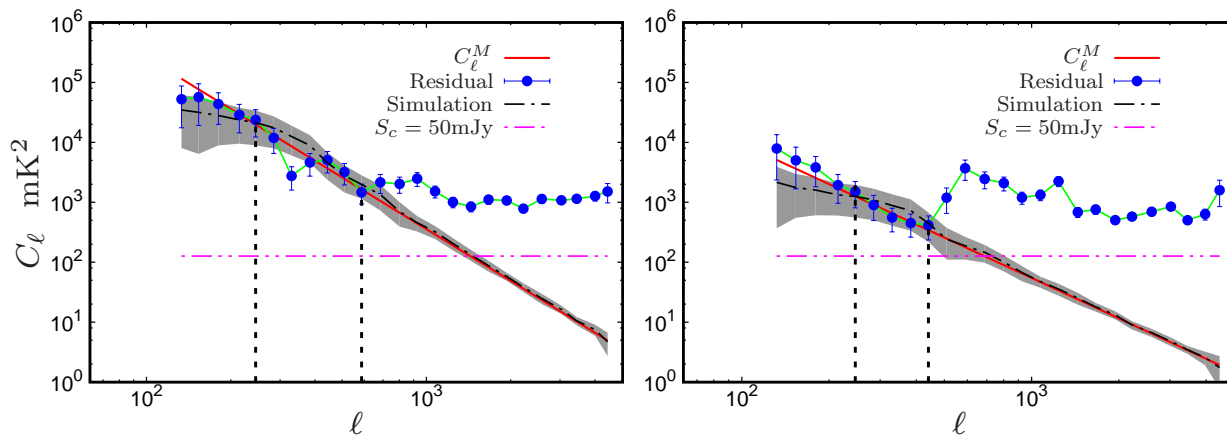


**Figure 3.** Estimated angular power spectra ( $C_\ell$ ) using residual data. The left and right panels refer to **Data1** and **Data2** respectively. The solid circles with  $1 - \sigma$  error bars show  $C_\ell$  estimated from the residual data, the vertical dashed lines show the  $\ell_{min} - \ell_{max}$  range used for fitting a power law model and the solid lines show the best fit model. The dash-dot lines with the  $1 - \sigma$  shaded region show the mean and standard deviation of  $C_\ell$  estimated from 128 realizations of simulations with the best fit power law as input model. The dot-dot-dash horizontal lines show  $C_\ell$  predicted from the residual point sources below a threshold flux density  $S_c = 50$  mJy. Note that, for **Data2** the estimated values are only upper limits on the DGSE power spectrum (see Section 3.)

fect subtraction of the bright sources possibly also makes a significant contribution in the measured  $C_\ell$  at large  $\ell$ . This interpretation is mainly guided by the model predictions (Figure 6 of Ali et al. 2008), and is also indicated by the nearly flat  $C_\ell$  which is consistent with the Poisson fluctuations of a random point source distribution. In contrast to this,  $C_\ell$  shows a steep power-law  $\ell$  dependence at small  $\ell$  ( $\leq \ell_{max}$ ) with  $\ell_{max} = 580$  and  $440$  for **Data1** and **Data2** respectively. This steep power law is the characteristic of the diffuse Galactic emission and we believe that the measured  $C_\ell$  is possibly dominated by the DGSE at the large angular scales corresponding to  $\ell \leq \ell_{max}$ . As mentioned earlier, the convolution in equation (3) is expected to be important at large angular scales and it is necessary to account for this in order to correctly interpret the results at small  $\ell$ .

We have carried out simulations in order to assess the effect of the convolution on the estimated  $C_\ell$ . GMRT visibility data was simulated assuming that the sky brightness temperature fluctuations are a realization of a Gaussian random field with input model angular power spectrum  $C_\ell^M$  of the form given by eq. (1). The simulations incorporate the GMRT primary beam pattern and the  $uv$  tracks corresponding to the actual observation under consideration. The reader is referred to Choudhuri et al. (2014) for more details of the simulations. Figure 2 shows the  $C_\ell$  estimated from the **Data1** simulations for  $\beta = 3$  and  $1.5$  which roughly encompasses the entire range of the power law index we expect for the Galactic synchrotron emission. We find that the effect of the convolution is important in the range  $\ell < \ell_{min} = 240$ , and we have excluded this  $\ell$  range from our analysis. We are, however, able to recover the input model angular power spectrum quite accurately in the region  $\ell \geq \ell_{min}$  which we have used for our subsequent analysis. We have also carried out the same analysis for **Data2** (not shown here) where we find that  $\ell_{min}$  has a value that is almost the same as for **Data1**.

We have used the  $\ell$  range  $\ell_{min} \leq \ell \leq \ell_{max}$  to fit a power law of the form given in eq. (1) to the  $C_\ell$  measured after point source subtraction. The data points with  $1 - \sigma$

error bars and the best fit power law are shown in Figure 3. Note that we have identified one of the **Data1** points as an outlier and excluded it from the fit. The best fit parameters ( $A, \beta$ ),  $N$  the number of data points used for the fit and  $\chi^2/(N - 2)$  the chi-square per degree of freedom (reduced  $\chi^2$ ) are listed in Table 1. The rather low values of the reduced  $\chi^2$  indicate that the errors in the measured  $C_\ell$  have possibly been somewhat overestimated. In order to validate our methodology we have simulated the visibility data for an input model power spectrum with the best fit values of the parameters ( $A, \beta$ ) and used this to estimate  $C_\ell$ . The mean  $C_\ell$  and  $1 - \sigma$  errors (shaded region) estimated from 128 realization of the simulation are shown in Figure 3. For the relevant  $\ell$  range we find that the simulated  $C_\ell$  is in very good agreement with the measured values thereby validating the entire fitting procedure. The horizontal lines in both the panels of Figure 3 show the  $C_\ell$  predicted from the Poisson fluctuations of residual point sources below a threshold flux density of  $S_c = 50$  mJy. The  $C_\ell$  prediction here is based on the 150 MHz source counts of Ghosh et al. (2012). We find that for  $\ell > \ell_{max}$  the measured  $C_\ell$  values are well in excess of this prediction indicating that (1.) there are significant residual imaging artifacts around the bright source ( $S > S_c$ ) which were subtracted, and/or (2.) the actual source distribution is in excess of the predictions of the source counts. Note that the actual  $S_c$  values (20.5 and 15.5 mJy for **Data1** and **Data2** respectively) are well below 50 mJy, and the corresponding  $C_\ell$  predictions will lie below the horizontal lines shown in Figure 3.

For both the fields  $C_\ell$  (Figure 3) is nearly flat at large  $\ell$  ( $> 500$ ) and it is well modeled by a power law at smaller  $\ell$  ( $240 \leq \ell \lesssim 500$ ). For **Data1** the power law rises above the flat  $C_\ell$ , and the power law is likely dominated by the DGSE. However, for **Data2** the power law falls below the flat  $C_\ell$ , and it is likely that in addition to the DGSE there is a significant residual point sources contribution. For **Data2** we interpret the best fit power law as an upper limit for the DGSE.

The best fit parameters  $(A, \beta) = (356.23 \pm 109.5, 2.8 \pm$



	Galactic Co-ordinate ( $l, b$ )	$\ell_{min}$	$\ell_{max}$	A (mK <sup>2</sup> )	$\beta$	$N$	$\chi^2/(N-2)$
<b>Data1</b>	(9°, +10°)	240	580	356 ± 109	2.8 ± 0.3	6 <sup>a</sup>	0.33
<b>Data2</b>	(15°, -11°)	240	440	54 ± 26	2.2 ± 0.4	5	0.15
Bernardi et al. 2009	(137°, +8°)	100	900	253 ± 40	2.2 ± 0.3	–	–
Ghosh et al. 2012	(151.8°, +13.89°)	253	800	513 ± 41	2.34 ± 0.28	–	–
Iacobelli et al. 2013	(137°, +7°)	100	1300	–	1.84 ± 0.19	–	–
La Porta et al. 2008	(-, ≥ +10°)	–	–	175 <sup>b</sup>	2.88	–	–
	(-, ≤ -10°)	–	–	212 <sup>b</sup>	2.74	–	–
	(-, ≥ +20°)	–	–	85 <sup>b</sup>	2.88	–	–
	(-, ≤ -20°)	–	–	50 <sup>b</sup>	2.83	–	–
	(-, ≥ +10°)	–	–	691 <sup>c</sup>	2.80	–	–
	(-, ≤ -10°)	–	–	620 <sup>c</sup>	2.70	–	–
	(-, ≥ +20°)	–	–	275 <sup>c</sup>	2.83	–	–
	(-, ≤ -20°)	–	–	107 <sup>c</sup>	2.87	–	–

**Table 1.** This shows the values of the parameters which are used to fit the data. In comparison, the parameters from other observations are also shown in this table. For **Data2**, the best fit values are derived with the assumption that the residual contribution is negligible below  $\ell_{max}$ .

<sup>a</sup> Excluding one outlier point; <sup>b</sup> Extrapolated from 1420 MHz to 147.5 MHz; <sup>c</sup> Extrapolated from 408 MHz to 147.5 MHz.

0.3) and  $(54.6 \pm 26, 2.2 \pm 0.4)$  for **Data1** and **Data2** respectively are compared with measurements from other 150 MHz observations such as Bernardi et al. (2009); Ghosh et al. (2012); Iacobelli et al. (2013) in Table 1. Further, we have also used an earlier work (La Porta et al. 2008) at higher frequencies (408 and 1420 MHz) to estimate and compare the amplitude of the angular power spectrum of the DGSE expected at our observing frequency. Using the best-fit parameters (tabulated at  $\ell = 100$ ) at 408 and 1420 MHz, we extrapolate the amplitude of the  $C_\ell$  at our observing frequency at  $\ell = 1000$  for  $|b| \geq 10^\circ$  and  $|b| \geq 20^\circ$ . In this extrapolation we use a mean frequency spectral index of  $\alpha = 2.5$  (de Oliveira-Costa et al. 2008) ( $C_\ell \propto \nu^{2\alpha}$ ). The extrapolated amplitude values are shown in Table 1. In Table 1, we note that the angular power spectra of the DGSE in the northern hemisphere are comparatively larger than that of the southern hemisphere. The best fit parameter  $A$  for **Data1**(**Data2**) agrees mostly with the extrapolated values obtained from  $b \geq +10^\circ$  ( $b \leq -10^\circ$ ) and  $b \geq +20^\circ$  ( $b \leq -20^\circ$ ) within a factor of about 2 (4). The best fit parameter  $\beta$  for **Data1** and **Data2** is within the range of 1.5-3.0 found by all the previous measurements at 150 MHz and higher frequencies.

The entire analysis here is based on the assumption that the DGSE is a Gaussian random field. This is possibly justified for the small patch of the sky under observation given that the diffuse emission is generated by a random processes like MHD turbulence. The estimated  $C_\ell$  remains unaffected even if this assumption breaks down, only the error estimates will be changed. We note that the parameters ( $A, \beta$ ) are varying significantly from field to field across the different direction in the sky. We plan to extend this analysis for the whole sky and study the variation of the amplitude ( $A$ ) and power law index ( $\beta$ ) of  $C_\ell$  using the full TGGs survey in future.

#### 4 ACKNOWLEDGEMENTS

We thank an anonymous referee for helpful comments. S. Choudhuri would like to acknowledge the University Grant Commission, India for providing financial support. AG would like acknowledge Postdoctoral Fellowship from the South African Square Kilometre Array Project for financial support. We thank the staff of the GMRT that made these observations possible. GMRT is run by the National Centre for Radio Astrophysics of the Tata Institute of Fundamental Research. We thank the staff of the GMRT that made these observations possible. GMRT is run by the National Centre for Radio Astrophysics of the Tata Institute of Fundamental Research.

#### References

- Ali, S. S., Bharadwaj, S., & Chengalur, J. N. 2008, MNRAS, 385, 2166  
 Bennett C.L., Hill R.S., Hinshaw. G. et al., 2003, ApJS, 148, 97  
 Bernardi, G., de Bruyn, A. G., Brentjens, M. A., et al. 2009, A & A, 500, 965  
 Bharadwaj, S., & Ali, S. S. 2005, MNRAS, 356, 1519  
 Bowman J. D. et al., 2013, PASA, 30, e031  
 Choudhuri, S., Bharadwaj, S., Ghosh, A., & Ali, S. S. 2014, MNRAS, 445, 4351  
 Choudhuri, S., Bharadwaj, S., Chatterjee, S., Ali, S. S., Roy, N., Ghosh, A., 2016, MNRAS, 463, 4093  
 Choudhuri, S., Bharadwaj, S., Roy, N., Ghosh, A., & Ali, S. S., 2016a, MNRAS, 459, 151  
 de Oliveira-Costa A., Tegmark M., Gaensler B. M., Jonas J., Landecker T. L., Reich P., 2008, MNRAS, 388, 247  
 Furlanetto, S. R., Oh, S. P., & Briggs, F. H. 2006, Physics Reports, 433, 181  
 Giardino, G., Banday, A. J., Fosalba, P., et al. 2001, A & A, 371, 708

- Giardino, G., Banday, A. J., Górski, K. M., et al. 2002, *A & A*, 387, 82
- Ghosh, A., Bharadwaj, S., Ali, S. S., & Chengalur, J. N. 2011a, *MNRAS*, 411, 2426
- Ghosh, A., Bharadwaj, S., Ali, S. S., & Chengalur, J. N. 2011b, *MNRAS*, 418, 2584
- Ghosh, A., Prasad, J., Bharadwaj, S., Ali, S. S., & Chengalur, J. N. 2012, *MNRAS*, 426, 3295
- Haslam, C. G. T., Salter, C. J., Stoffel, H., & Wilson, W. E. 1982, *A&AS* 47, 1
- Iacobelli, M., Haverkorn, M., Orrú, E., et al. 2013, *A & A*, 558, A72
- Intema, H. T., van der Tol, S., Cotton, W. D., et al. 2009, *A & A*, 501, 1185
- Intema, H. T. 2014, arXiv:1402.4889
- Intema, H. T., Jagannathan, P., Mooley, K. P., & Frail, D. A. 2016, arXiv:1603.04368
- Koopmans, L., Pritchard, J., Mellema, G., et al. 2015, *Advancing Astrophysics with the SKA (AASKA14)*, 1
- La Porta, L., Burigana, C., Reich, W., & Reich, P. 2008, *A & A*, 479, 641
- Lazarian, A., & Pogosyan, D. 2012, *ApJ*, 747, 5
- Morales, M. F., & Wyithe, J. S. B. 2010, *ARAA*, 48, 127
- Neben, A. R., Bradley, R. F., Hewitt, J. N., et al. 2016, *ApJ*, 826, 199
- Parsons A. R. et al., 2010, *AJ*, 139, 1468
- Pritchard, J. R., & Loeb, A. 2012, *Reports on Progress in Physics*, 75, 086901
- Reich, W. 1982, *A&AS* 48, 219
- Reich, P., & Reich, W. 1988, *A&AS*, 74, 7
- Shaver, P. A., Windhorst, R. A., Madau, P., & de Bruyn, A. G. 1999, *A & A*, 345, 380
- Sirothia, S. K., Lecavelier des Etangs, A., Gopal-Krishna, Kantharia, N. G., & Ishwar-Chandra, C. H. 2014, *A & A*, 562, A108
- Swarup, G., Ananthakrishnan, S., Kapahi, V. K., Rao, A. P., Subrahmanya, C. R., and Kulkarni, V. K. 1991, *CURRENT SCIENCE*, 60, 95.
- van Haarlem, M. P., Wise, M. W., Gunst, A. W., et al. 2013, *A & A*, 556, A2
- Waelkens, A. H., Schekochihin, A. A., & Enßlin, T. A. 2009, *MNRAS*, 398, 1970